Reconfigurable wave band structure of an artificial square ice

Ezio Iacocca, Sebastian Gliga, Robert L. Stamps, and Olle Heinonen

Phys. Rev. B **93**, 134420 — Published 18 April 2016

DOI: 10.1103/PhysRevB.93.134420

Reconfigurable spin wave band structure of artificial square spin ice

Ezio Iacocca,[1,2,3,*] Sebastian Gliga,[4,5] Robert L. Stamps,[6] and Olle Heinonen[7,8]

[1] *Department of Applied Mathematics, University of Colorado, Boulder, Colorado 80309-0526, USA*
[2] *Department of Applied Physics, Division for condensed matter theory, Chalmers University of Technology, 412 96, Gothenburg, Sweden*
[3] *Physics Department, University of Gothenburg, 412 96, Gothenburg, Sweden*
[4] *Laboratory for Mesoscopic Systems, Department of Materials, ETH Zurich, 8093 Zurich, Switzerland*
[5] *Laboratory for Micro- and Nanotechnology, Paul Scherrer Institute, 5232 Villigen PSI, Switzerland*
[6] *School of Physics and Astronomy, University of Glasgow, Glasgow, UK, G12 8QQ*
[7] *Materials Science Division, Argonne National Laboratory, Lemont, IL 60439, USA*
[8] *Northwestern-Argonne Institute for Science and Engineering, Evanston, IL 60208, USA*

Artificial square spin ices are structures composed of magnetic elements arranged on a geometrically frustrated lattice and located on the sites of a two-dimensional square lattice, such that there are four interacting magnetic elements at each vertex. Using a semi-analytical approach, we show that square spin ices exhibit a rich spin wave band structure that is tunable both by external magnetic fields and the configuration of individual elements. Internal degrees of freedom can give rise to equilibrium states with bent magnetization at the edges leading to characteristic excitations; in the presence of magnetostatic interactions these form separate bands analogous to impurity bands in semiconductors. Full-scale micromagnetic simulations corroborate our semi-analytical approach. Our results show that artificial square spin ices can be viewed as reconfigurable and tunable magnonic crystals that can be used as metamaterials for spin-wave-based applications at the nanoscale.

Spin waves, or magnons, are fundamental excitations in magnetic thin films and nanostructures. Because of their potential applications in information technology[1,2] and computation[3], means to control magnon dispersion and band gap have been studied intensively over the past few decades. The term *magnonics* has been coined to describe this field of study[4,5]. One pathway to control magnon dispersions is to construct magnonic crystals[6,7] that are metamaterials with a spatial modulation of the magnetic properties on length scales comparable to relevant magnonic wavelengths[8–10]. Patterned thin magnetic films[11,12] or topographically modulated thin films have been used to manipulate the magnon spectra[13]. This approach is similar to super-lattices in photonics and, fundamentally, to the crystal structure of semiconductors. A paradigm that is the focus of recent investigation consists in actively modifying the band structure of magnonic crystals[14]. This has been achieved to date by use of Meander-type structures[15] and, more recently, via heating[16] in one-dimensional ferromagnets.

Artificial spin ices[17–19] are another class of structures based on an organized array of nanosized magnetic elements that have been shown to support a wealth of static, dynamic, and emergent magnetic phenomena[19–21]. Artificial spin ices are geometrically *frustrated*: the geometry of the elements and the lattice are such that all interaction energies cannot be simultaneously minimized. Examples of artificial spin ices are the square ice[17], and the kagome ice[22]. The square ice is composed of magnetic stadium-shaped nanoislands positioned on the sites of a two-dimensional square lattice with lattice constant d, Fig. 1(a), and obeys the "ice rules" in which low-energy states are characterized by the magnetization in two islands pointing into a vertex and out of the vertex in the two other nanoislands. Dynamically, correlated excitations are supported in spin ices because of the magnetostatic interactions between magnetic islands[23]. Because of their intrinsic periodicity and wealth of static states, artificial spin ices offer interesting opportunities as programmable magnonic crystals to control the magnon dispersion and band gap [19].

The resonant mode spectrum of square ices has been studied numerically by means of micromagnetic simulations, demonstrating the observable effects of magnetic defects[23]. More recently, a detailed numerical study has shown that edge modes arising from the internal degrees of freedom equally have observable consequences in the resonant spectrum in sufficiently thick nanoislands[24]. In fact, edge modes efficiently couple neighboring nanoislands, influencing the collective oscillations[19]. This is reminiscent of impurity states in semiconductors that locally modify the energy landscape and give rise to shallow electronic bands[25]. Recent experimental results have explored the excitation spectrum of artificial spin ices[26–28] but the existence and dependencies of the band diagram in square ices has not been explored to date. To close the gap between the fields magnonics and artificial spin ices, we examine square ices from the perspective of magnonics, including bands arising from the edge modes as well as the bulk modes.

In this Rapid Communication, we study long-range dipolar-mediated two-dimensional magnon dispersion in square ices in the spirit of a tight-binding model. In contrast to similar procedures on simpler structures[29,30], we account for the internal degrees of freedom resulting from edge modes in the nanoislands. Consequently, we are able to calculate the magnon dispersion as a function of local equilibrium states as well as its field tunability, including edge mode bands. Our semi-analytical approach provides enough degrees of freedom to qualitatively estimate the

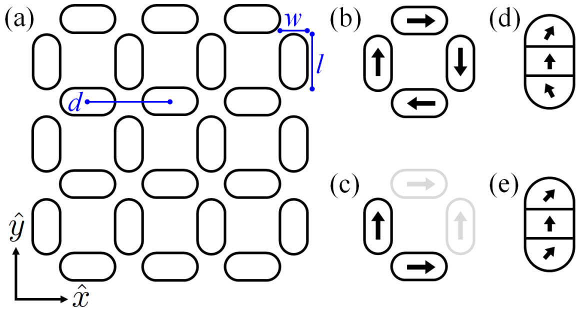

FIG. 1. (Color online) (a) Square ice lattice with lattice constant d, and with magnetic stadia of width w, length l, and thickness t. The stable magnetization directions (black arrows) of the magnetic elements in a unit cell are shown for the (b) ground (vortex) and (c) remanent state (the gray-colored stadia are not part of the unit cell and are shown here for clarity). Edge states have two stable configurations as (d) C and (e) S states.

band structure of an extended square ice lattice while being computationally tractable.

We focus on the small-amplitude excitations in two energetically stable configurations of a square ice, namely the vortex and remanent states, Fig. 1(b) and (c), respectively. The vortex state is the ground state of the system, achieved by thermal relaxation[31], and the remanent state can be obtained by saturating the system in an external field along the $(\hat{x}, \hat{y})$ direction, and then slowly removing the external field, letting the system relax. In each configuration, the magnetization can bend close to the nanoisland edges[24], providing a local "impurity". In square ices, two stable edge configurations satisfy the minimization of dipolar fields at the ground state, resulting in C and S states[32–34], Fig. 1(d)-(e).

The small-amplitude dynamics in square ices can be approached semi-analytically using a Hamiltonian formalism[35]. The same approach has been used and shown to be accurate in many dynamical regimes to date[36–42]. In this formalism, the Landau-Lifshitz equation of motion describing conservative magnetization dynamics is cast as a function of a complex amplitude a, using a Holstein-Primakoff transformation. By expanding the resulting equation in Taylor series, the linear dynamics for an ensemble of complex amplitudes $\underline{a}$ can be generally expressed (see Supplementary material) as

$$\frac{d\underline{a}}{dt} = -i\frac{d}{d\underline{a}^*}\underline{A}^\dagger \mathcal{H}\underline{A} = -i\frac{d}{d\underline{a}^*}\underline{A}^\dagger \begin{pmatrix} \mathcal{H}^{(1,1)} & \mathcal{H}^{(1,2)} \\ \mathcal{H}^{(2,1)} & \mathcal{H}^{(2,2)} \end{pmatrix} \underline{A}, \quad (1)$$

where the dagger denotes the complex transpose, $\underline{A}$ is an array of $2n$ complex amplitudes $\underline{A}^T = [\underline{a}^T, \underline{a}^\dagger] = [a_1, ..., a_n, a_1^*, ..., a_n^*]$ and $\mathcal{H}$ is the $2n \times 2n$ Hamiltonian. The right-hand-side of Eq. (1) includes terms up to second order in $\underline{a}$, corresponding to linear excitations. Beacuse of the lattice perodicity, propagating waves are Bloch waves with a time dependence gvien by $a \to ae^{i\omega t}$. This allows us to reduce Eq. (1) to an eigenvalue problem by means of Colpa's grand dynamical matrix[43]

$$\omega\underline{\psi} = \begin{pmatrix} \mathcal{H}^{(1,2)} & \mathcal{H}^{(2,2)} \\ \mathcal{H}^{(1,1)} & \mathcal{H}^{(2,1)} \end{pmatrix} \underline{\psi}, \quad (2)$$

from which we obtain the eigenvalues ω, and the eigenvectors $\underline{\psi}$. Due to the complex conjugate definition of $\underline{A}$, we observe that $\mathcal{H}^{(1,1)} = \mathcal{H}^{(2,2)}$ and $\mathcal{H}^{(1,2)} = \mathcal{H}^{(2,1)}$, leading to conjugate eigenvalues in Eq. (2).

The Hamiltonian is related to the magnetic field $\vec{H}$ via $\mathcal{H} = -\gamma\delta W/(2M_S)$, where $\delta W = -\int \vec{H}(\vec{M}) \cdot d\vec{M}$ is the energy functional, γ is the gyromagnetic ratio, $\vec{M}$ is the magnetization vector, and $M_S = ||\vec{M}||$ is the saturation magnetization. We consider field contributions from shape anisotropy, dipolar interactions, and intra-element exchange as well as an external applied field. Each field contribution can be reduced to a Hamiltonian matrix as detailed in the Supplementary material. Of particular importance are the dipolar interactions, which are the only source of inter-element coupling in our framework and the concomitant magnon dispersion. The dipolar energy between a nanoisland j in cell τ and all the other nanoislands k in cells τ' can be expressed as

$$\mathcal{H}_d = -\frac{V}{4\pi}\sum_{k,\tau'}\Big[\frac{3(\vec{R}_{jk,\tau\tau'}\cdot\vec{M}_{j,\tau'})(\vec{R}_{jk,\tau\tau'}\cdot\vec{M}_{j,\tau})}{(\vec{R}_{jk,\tau\tau'})^5} - \frac{\vec{M}_{j,\tau'}\cdot\vec{M}_{j,\tau}}{(\vec{R}_{jk,\tau\tau'})^3}\Big], \quad (3)$$

where V is the volume of the magnetic element and $\vec{R}_{jk,\tau\tau'}$ is the translation vector between the nanoisland j in cell τ and the nanoisland k in cell τ'. Considering the Bloch wave $\vec{M}_{j,\tau} = \vec{M}_{j,\tau'}e^{i\vec{q}\vec{R}_{jk}}$, where $\vec{q}$ is the wave vector, it is possible to recast Eq. (3) for the unit cell in terms of the lattice (S_β where $\beta = \hat{x}, \hat{y}, \hat{z}$) and cross-direction ($S_c$) summations. As an example, the resulting Hamiltonian matrices for the ground state in the absence of exchange interactions are

$$\mathcal{H}_d^{(1,1)} = \begin{pmatrix} S_x^{11} & S_c^{12} & S_x^{13} & S_c^{14} \\ S_c^{21} & S_y^{22} & S_c^{23} & S_y^{24} \\ S_x^{31} & S_c^{23} & S_x^{33} & S_c^{34} \\ S_c^{41} & S_y^{24} & S_c^{34} & S_y^{44} \end{pmatrix} - \hat{S}_z \quad (4a)$$

$$\mathcal{H}_d^{(1,2)} = \mathcal{D} + \begin{pmatrix} 0 & S_c^{12} & S_x^{13} & S_c^{14} \\ S_c^{21} & 0 & S_c^{23} & S_y^{24} \\ S_x^{31} & S_c^{32} & 0 & S_c^{34} \\ S_c^{41} & S_y^{42} & S_c^{43} & 0 \end{pmatrix} + \hat{S}_z, \quad (4b)$$

where $\mathcal{D}$ is a diagonal matrix containing inter-island interactions (the expressions for $\mathcal{D}$ and the lattice summations are shown in the Supplementary material). The reduction of the dipolar field to Hamiltonian matrices is a key result of this work.

The magnon dispersion can be numerically calculated by solving the eigenvalue problem of Eq. (2). We consider a square ice composed of Permalloy stadia with

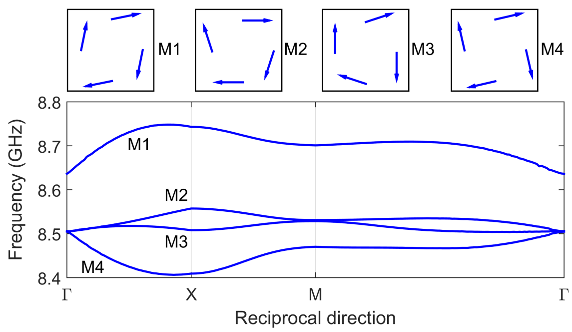

FIG. 2. (Color online) Band structure of the vortex state. The insets show the magnetization vector configuration of the unit cell for each band, showcasing their excitation symmetry.

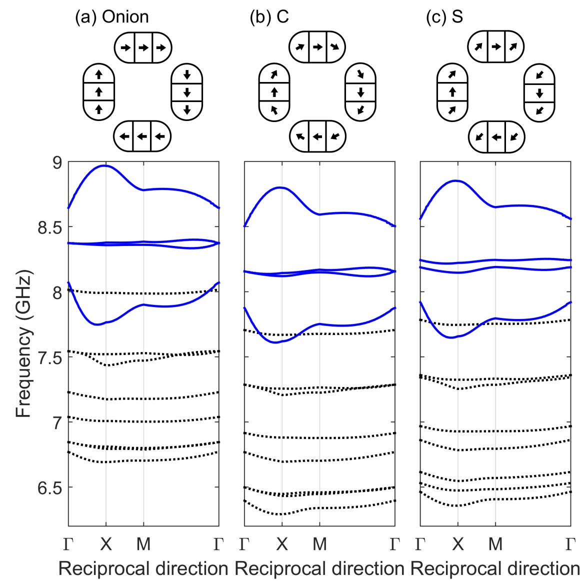

FIG. 3. (Color online) Band diagram for the vortex state in a (a) onion, (b) C, and (c) S state. The bulk (edge) modes are depicted in blue (dashed black) lines. The schematic of each static configuration is also shown for each case.

dimensions 280 nm$\times$ 120 nm$\times$ 20 nm, saturation magnetization $M_S = 770$ kA/m, and center-to-center separation of $d = 395$ nm. Exchange is implemented as an additional degree of freedom in a nanoisland divided by three equidistant spins coupled by the constant $J = 0.016$, which parametrizes the exchange in Permalloy $J = cA/2$, where $c = 0.33$ nm is the lattice constant and $A = 10$ pJ/m is the exchange stiffness. This approximation for the exchange interaction is applicable for the low-energy sector of the magnon bands, as demonstrated below by the good quantitative agreement with full-scale micromagnetic simulations.

It is instructive to consider first the band structure neglecting internal degrees of freedom, or "macrospin" approximation. A typical band structure for the macrospin vortex state is shown in Fig. 2. There are four bands consistent with the available degrees of freedom in the system, one for each island. From the corresponding eigenvectors, it is possible to identify the location and symmetry of each mode. A snapshot of the magnetic configurations at the Γ point for each band (labeled from M1 to M4) are shown above Fig. 2. We notice that M1 has pair of islands in phase and a phase difference of $\pm\pi$ between each pair, whereas M4 represents a mode with all islands excited in phase. Furthermore, M1 (M4) has positive (negative) group velocity. M2 and M3 are close in energy and consist of modes with a pairwise phase difference of $\pm\pi/2$. Note that the pairwise difference make these bands non-degenerate, resulting in anti-crossings close to the Γ and M points. These latter two modes form narrow bands that separate away form the Γ point, and establish a band gap reaching ≈ 195 MHz between the Γ and X point of M1 and M2, respectively. Bands effectively touch at the Γ and M points. However, we did not observe band inversion in any calculation.

We now include exchange interactions in our framework. By dividing each magnetic island into three equidistant spins, we now have access to 12 bands. In the ground state, three configurations are stable: homogeneous or onion[24], C, and S states. The corresponding band diagrams are shown in Fig. 3. The additional degrees of freedom give rise to lower frequency bands identified as edge modes (black dashed lines), also showing anti-crossing behavior. We observe that the bulk modes (blue lines) maintain their qualitative features. However, the bandgaps are enhanced due to the additional energy incorporated into the system. Furthermore, the particular magnetic configuration quantitatively modifies the band diagram, indicating that edge bending can be compared to impurity states in semiconductor materials. Because a transition between C and S states can be induced by, *e.g.,* temperature[24], this can be used as another avenue to program the magnonic response of the square ice. In the remanent state, the unit cell is composed of two magnetic islands, Fig. 1(c). The band diagrams for a macrospin and stable onion and S configurations are shown in Fig. 4, exhibiting similar features as discussed above.

We now explore the effect of an applied field $\vec{H}_e$ on the square ice. We consider a feasible experimental scenario of an in-plane field along the $\hat{x}$ direction and detection of coherent excitations (at the Γ point) by means of resonance measurements (The effect of field angle is shown in the Supplementary material). Note that in our framework, the stable magnetization direction of the magnetic nanoislands is set and assumed *a priori*, *i.e.*, only small amplitude variations are accessible. In fact, large fields induce imaginary eigenvalues, denoting decaying modes and thus the breakdown of our model. We study the effect of field magnitudes between $0 < |\vec{H}_e| < 100$ Oe which maintains real eigenvalues. The results obtained for both vortex and remanent states under macrospin approximation are shown in Fig. 5(a-b). In the case of the vortex state, we observe that the coherent modes, M1

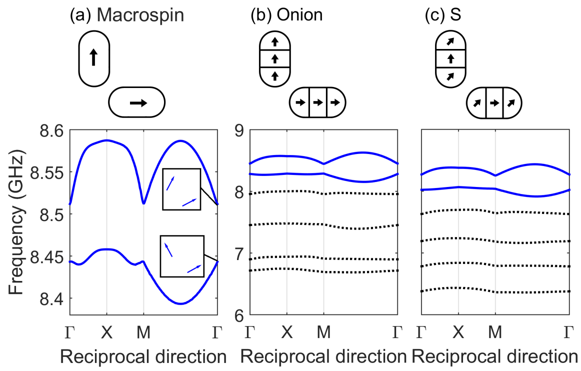

FIG. 4. (Color online) Band diagram for the remanent state in a (a) macrospin, (b) onion, and (c) S states. The bulk (edge) modes are depicted in blue (dashed black) lines. The inset shows the magnetization vector configuration of the unit cell for each band. The schematic of each static configuration is also shown for each case.

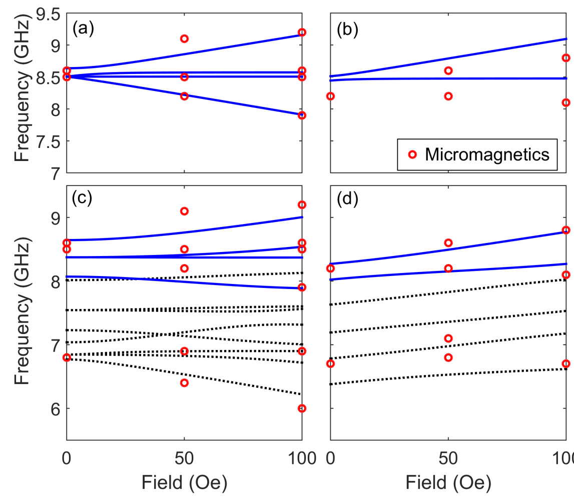

FIG. 5. (Color online) Magnon frequencies at the Γ point as a function of an external field applied along the $\hat{x}$ axis for the (a) macrospin vortex, (b) macrospin remanent, (c) onion vortex, and (d) remanent S states. The bulk (edge) modes are depicted in blue (dashed black) lines. The red dots are obtained from micromagnetic simulations.

and M4, have positive and negative tunabilities, respectively, whereas M2 and M3 exhibit only slight tunability. In the case of the remanent state we observe either a positive or negligible tunability. The strongly tunable modes can be traced to those magnetic elements parallel to the applied field. This is also consistent with the Landau-Lifshitz equation predicting a blue (red) shift of frequencies when the *internal* field increases (decreases). The modes with negligible tunability correspond to magnetic elements perpendicular to the field. By considering edge bending, a richer behavior for the tunability of both the vortex and remanent states is obtained, Fig. 5(c-d). For both the vortex in an onion state and the remanent S state, we observe similar tunabilities for the bulk and low-frequency edge modes. In all cases, the slope of each band is generally different, leading to band crossings, and implying that the bandgaps in square ices can be manipulated by an applied magnetic field.

Full-scale micromagnetic simulations were performed for comparison with the semi-analytical model. We used a computational system containing eight islands and imposing periodic boundary conditions consistent with the geometry described above (see Supplemental Material for details). The results are shown as red circles in Fig. 5 (note that the micromagnetic modeling only returns modes that are even in the unit cell because the exciting field is uniform, while the semi-analytical model captures all modes irrespective of symmetry). For the vortex state, a good agreement for the bulk modes is obtained from the macrospin model. Further comparison with the extended semi-analytical model also shows excellent agreement with the low-frequency edge modes. For the remanent state, the macrospin model yields a good qualitative agreement with the micromagnetic results. A three-spin S-state model also yields good agreement with the micromagnetic low-frequency modes, especially in view of the simplistic treatment in the three-spin model of the smooth static equilibrium magnetization in the micromagnetic model.

We remark that in both real and micromagnetically-modeled nanoislands, there are many higher-order modes, beyond what can be described by the three-spin model considered here, because of the many internal degrees of freedom. Such higher-order modes have many internal nodal lines of the magnetization eigenmodes. Therefore, the magnetostatic fields emanating from such modes decay rather quickly in space. This results in a weak coupling between different islands so the magnonic bands arising from such modes are non-dispersive with no phase or group velocity, and are not interesting here. It is also noteworthy that a strong variation of the islands aspect ratio can significantly affect the excited frequencies, *i.e.*, in the nanowire and circular dot limits. Moreover, we expect the thickness to play an important role in the ultra-thin film regime, where the anisotropy becomes perpendicular or can favor a vortex state inside each stadium.

In summary, we have calculated the magnon band structure and the mode tunability at the Γ point for a square ice in two equilibrium states, the vortex (or ground) state, and the remanent state, using a model that includes internal degrees of freedom of the islands as well as edge bending. The good quantitative agreement with micromagnetic simulations confirms the accuracy of the small-amplitude semi-analytical model while avoiding the computational limitations intrinsic to fully three-dimensional micromagnetic simulations. These results show that the magnon spectra, and therefore group and phase velocities as well as band gap, can be manipulated by external fields. In particular, the edge modes give rise to separate magnon bands allowing for a larger parameter space in terms of magnon control. This suggests that square ices can be considered metamaterials for spin waves. In addition, the square ice is in principle reconfigurable in that the magnetization in individual islands can be changed by the application of external fields (*e.g.,* from vortex to remanent state) or temperature, or by using more sophisticated techniques such as using spin torque by patterning nanocontacts on the elements or making the elements part of magnetic tunnel junctions. This opens up the possibility of two-dimensional reprogrammable magnonic crystals comprised of an artificial square spin ice.

ACKNOWLEDGMENTS

E. I. acknowledges support from the Swedish Research Council, Reg. No. 637-2014-6863. The work by O. H. was funded by the Department of Energy Office of Science, Materials Sciences and Engineering Division. E. I. was partly supported by the U.S. Department of Energy, Office of Science, Materials Sciences and Engineering Division through the Materials Theory Institute. We gratefully acknowledge the computing resources provided on Blues, a high-performance computing cluster operated by the Laboratory Computing Resource Center at Argonne National Laboratory. The work by R. L. S. was funded by EPSRC EP/L002922/1.

* ezio.iacocca@colorado.edu

[1] M. P. Kostylev, A. A. Serga, T. Schneider, B. Leven, and B. Hillebrands, Applied Physics Letters **87**, 153501 (2005).
[2] A. Khitun and K. L. Wang, Superlattices and Microstructures **38**, 184 (2005).
[3] A. V. Chumak, A. A. Serga, and B. Hillebrands, Nature Communications **5** (2013).
[4] S. Demokritov and A. Slavin, eds., *Magnonics From Fundamentals to Applications* (Springer, 2013).
[5] M. Krawczyk and D. Grundler, Journal of Physics: Condensed Matter **26**, 123202 (2014).
[6] S. Nikitov, P. Tailhades, and C. Tsai, Journal of Magnetism and Magnetic Materials **236**, 320 (2001).
[7] S. Neusser and D. Grundler, Advanced Materials **21**, 2927 (2009).
[8] Z. Wang, V. Zhang, H. Lim, S. Ng, M. Kuok, S. Jain, and A. Adeyeye, ACS Nano **4**, 643 (2010).
[9] S. Tacchi, F. Montoncello, M. Madami, G. Gubbiotti, G. Carlotti, L. Giovannini, R. Zivieri, F. Nizzoli, S. Jain, A. O. Adeyeye, and N. Singh, Phys. Rev. Lett. **107**, 127204 (2011).
[10] S. Tacchi, G. Duerr, J. W. Klos, M. Madami, S. Neusser, G. Gubbiotti, G. Carlotti, M. Krawczyk, and D. Grundler, Phys. Rev. Lett. **109**, 137202 (2012).
[11] V. V. Kruglyak, S. O. Demokritov, and D. Grundler, J. Phys. D: Appl. Phys. **43**, 264001 (2010).
[12] B. Lenk, H. Ulrichs, F. Garbs, and M. Münzenberg, Physics Reports **507**, 107 (2011).
[13] J. Sklenar, P. Tucciarone, R. J. Lee, D. Tice, R. P. H. Chang, S. J. Lee, I. P. Nevirkovets, O. Heinonen, and J. B. Ketterson, Phys. Rev. B **91**, 134424 (2015).
[14] D. Grundler, Nature Physics **11**, 438 (2015).
[15] A. D. Karenowska, J. F. Gregg, V. S. Tiberkevich, A. N. Slavin, A. V. Chumak, A. A. Serga, and B. Hillebrands, Phys. Rev. Lett. **108**, 015505 (2012).
[16] M. Vogel, A. V. Chumak, E. H. Waller, T. Langner, V. I. Vasyuchka, B. Hillebrands, and G. von Freymann, Nature Physics **11** (2015).
[17] R. Wang, C. Nisoli, R. Freitas, J. Li, W. McConville, B. Cooley, M. Lund, N. Samarth, C. Leighton, V. Crespi, and P. Schiffer, Nature **439**, 303 (2005).
[18] C. Nisoli, R. Moessner, and P. Schiffer, Rev. Mod. Phys. **85**, 1473 (2013).
[19] L. J. Heyderman and R. L. Stamps, Journal of Physics: Condensed Matter **25**, 363201 (2013).
[20] R. L. Stamps, S. Breitkreutz, J. Åkerman, A. V. Chumak, Y. Otani, G. E. W. Bauer, J.-U. Thiele, M. Bowen, S. A. Majetich, M. Kläui, I. L. Prejbeanu, B. Dieny, N. M. Dempsey, and B. Hillebrands, Journal of Physics D: Applied Physics **47**, 33 (2014).
[21] V. Kapaklis, U. Arnalds, A. Farhan, R. Chopdekar, A. Balan, A. Scholl, L. Heyderman, and B. Hjörvarsson, Nature Nanotechnology (2014).
[22] Y. Qi, T. Brintlinger, and J. Cumings, Phys. Rev. B **77**, 094418 (2008).
[23] S. Gliga, A. Kákay, R. Hertel, and O. G. Heinonen, Phys. Rev. Lett. **110**, 117205 (2013).
[24] S. Gliga, A. Kákay, L. J. Heyderman, R. Hertel, and O. G. Heinonen, Phys. Rev. B **92**, 060413 (2015).
[25] M. Balkanski and R. Wallis, *Semiconductor physics and applications* (Oxford University Press, 2000).
[26] M. B. Jungfleisch, W. Zhang, E. Iacocca, J. Sklenar, J. Ding, W. Jiang, S. Zhang, J. E. Pearson, V. Novosad, J. B. Ketterson, O. Heinonen, and A. Hoffmann, Phys. Rev. B **93**, 100401 (2016).
[27] V. S. Bhat, F. Heimbach, I. Stasinopoulos, and D. Grundler, **arXiv:1602.00918** (2016).
[28] X. Zhou, G.-L. Chua, N. Singh, and A. O. Adeyeye, Adv. Func. Mater. (2016), 10.1002/adfm.201505165.
[29] R. Shindou, R. Matsumoto, S. Murakami, and J.-i. Ohe, Phys. Rev. B **87**, 174427 (2013).
[30] R. Shindou, J.-i. Ohe, R. Matsumoto, S. Murakami, and E. Saitoh, Phys. Rev. B **87**, 174402 (2013).
[31] A. Farhan, P. M. Derlet, A. Kleibert, A. Balan, R. V. Chopdekar, M. Wyss, J. Perron, A. Scholl, F. Nolting, and L. J. Heyderman, Phys. Rev. Lett. **111**, 057204 (2013).
[32] R. P. Cowburn, Journal of Physics D: Applied Physics **33**, R1 (2000).
[33] M. Madami, G. Carlotti, G. Gubbiotti, F. Scarponi, S. Tacchi, and T. Ono, Journal of Applied Physics **109**, 07B901 (2011).
[34] G. Carlotti, G. Gubbiotti, M. Madami, S. Tacchi, F. Hart-

mann, M. Emmerling, M. Kamp, and L. Worschech, Journal of Physics D: Applied Physics **47**, 265001 (2014).
[35] A. Slavin and V. Tiberkevich, Magnetics, IEEE Transactions on **45**, 1875 (2009).
[36] A. Slavin and V. Tiberkevich, Phys. Rev. Lett. **95**, 237201 (2005).
[37] S. Bonetti, V. Tiberkevich, G. Consolo, G. Finocchio, P. Muduli, F. Mancoff, A. Slavin, and J. Åkerman, Phys. Rev. Lett. **105**, 217204 (2010).
[38] E. Iacocca and J. Åkerman, Phys. Rev. B **85**, 184420 (2012).
[39] E. Iacocca and J. Åkerman, Phys. Rev. B **87**, 214428 (2013).
[40] E. Iacocca, O. Heinonen, P. K. Muduli, and J. Åkerman, Phys. Rev. B **89**, 054402 (2014).
[41] E. Iacocca, P. Dürrenfeld, O. Heinonen, J. Åkerman, and R. K. Dumas, Phys. Rev. B **91**, 104405 (2015).
[42] N. Locatelli, A. Hamadeh, F. Abreu Araujo, A. D. Belanovsky, P. N. Skirdkov, R. Lebrun, V. V. Naletov, K. Zvezdin, M. M, J. Grollier, O. Klein, V. Cros, and G. de Loubens, arXiv:1506.03603v1 (2015).
[43] J. Colpa, Physica A: Statistical Mechanics and its Applications **93**, 327 (1978).